

Transition parameters of Li-like ions (Z=7-11) in dense plasmas

Xiang-Fu Li(李向富), Li-Ping Jia(贾利平), Hong-Bin Wang(王宏斌), Gang Jiang(蒋刚)
Citation: Chin. Phys. B, 2021, 30 (**5**): 053102. DOI: 10.1088/1674-1056/abea80
Journal homepage: http://cpb.iphy.ac.cn; http://iopscience.iop.org/cpb

What follows is a list of articles you may be interested in

Analytical expressions of non-relativistic static multipole polarizabilities for hydrogen-like ions

Xuesong Mei(梅雪松), Wanping Zhou(周挽平), Zhenxiang Zhong(钟振祥), Haoxue Qiao(乔豪学)
Chin. Phys. B, 2020, 29 (**4**): 043101. DOI: 10.1088/1674-1056/ab75d0

Vibronic spectra of aluminium monochloride relevant to circumstellar molecule

Jian-Gang Xu(徐建刚), Cong-Ying Zhang(张聪颖), Yun-Guang Zhang(张云光)
Chin. Phys. B, 2020, 29 (**3**): 033102. DOI: 10.1088/1674-1056/ab6c46

Study of highly excited vibrational dynamics of HCP integrable system with dynamic potential methods

Aixing Wang(王爱星), Lifeng Sun(孙立风), Chao Fang(房超), Yibao Liu(刘义保)
Chin. Phys. B, 2020, 29 (**1**): 013101. DOI: 10.1088/1674-1056/ab593a

Relativistic calculations of fine-structure energy levels of He-like Ar in dense plasmas

Xiang-Fu Li(李向富), Gang Jiang(蒋刚)
Chin. Phys. B, 2018, 27 (**7**): 073101. DOI: 10.1088/1674-1056/27/7/073101

Isotope shift calculations for D lines of stable and short-lived lithium nuclei

Geng-Hua Yu(余庚华), Peng-Yi Zhao(赵朋义), Bing-Ming Xu(徐炳明), Wei Yang(杨维), Xiao-Ling Zhu(朱晓玲)
Chin. Phys. B, 2016, 25 (**11**): 113102. DOI: 10.1088/1674-1056/25/11/113102

Transition parameters of Li-like ions ($Z = 7$–11) in dense plasmas*

Xiang-Fu Li(李向富)[1,†], Li-Ping Jia(贾利平)[1], Hong-Bin Wang(王宏斌)[2], and Gang Jiang(蒋刚)[3]

[1] College of Electrical Engineering, Longdong University, Qingyang 745000, China
[2] College of Science, Xi'an University of Posts & Telecommunications, Xi'an 710121, China
[3] Institute of Atomic and Molecular Physics, Sichuan University, Chengdu 610065, China

(Received 13 October 2020; revised manuscript received 7 February 2021; accepted manuscript online 1 March 2021)

The energy levels, transition energies, transition probabilities, weighted oscillator strengths, and line strengths of Li-like ions ($Z = 7$–11) in dense plasmas are investigated in this work. The relativistic effects and electron correlation effects are described by the MCDHF method. The ion sphere model is applied to include the dense plasma screening effect. The ground configuration $1s^22s$ and the excited $1s^22p$, $1s^23l$ ($l = 0$–2) are considered. The configuration sets are enlarged until $n = 7$ where the calculated energy levels have converged. The critical free electron densities of $1s^23d$ states are estimated. Except for $1s^23s$–$1s^23p$ transitions, the transition energies for $\Delta n = 0$ increase, and for $\Delta n \neq 0$ decrease with increasing free electron densities. For $1s^23s$–$1s^23p$ transitions, the spectra show blue-shift at lower free electron densities and red-shift at higher free electron densities, and the energy level crossing phenomens are observed at higher free electron densities.

Keywords: Li-like ions, energy levels, transition energies, transition probabilities

PACS: 31.15.ac, 31.15.ag, 31.15.xr, 52.27.Gr **DOI:** 10.1088/1674-1056/abea80

1. Introduction

In dense plasma environments, the interaction between the electrons with atomic nucleus is screened, as well as that between electrons. Electronic structures of atomic systems immersed in dense plasma environment may be remarkably different from their corresponding isolated candidates.[1] Many interesting phenomena have been observed in dense plasmas, such as spectral line shift, broadening of spectral lines, line merging, and so on.[2] Apart from its fundamental importance, the study of atomic structure in plasma environments has practical implications in many fields of science, such as atomic physics in dense plasmas including the famous ionization potential depression (IPD), inertial confinement fusion research, laser produced plasmas, astrophysics, plasma equation of state (EOS), plasma fluid, particle simulations and opacity.[3–5]

Although several dense plasma experiments[6–10] have been performed recently by intense short-pulse laser irradiation, the results of these experiments are controversial. The measured IPDs of experiment[6] are in line with the description of Stewart and Pyatt model,[11] but that of experiments[7–9] show that Stewart and Pyatt model[11] underestimates the IPD, and are more consistent with Ecker–Kröell model.[12] The proof-of-principle experiment[10] performed at LCLS shows that it is still need highly precise measurements of the ionization potential to end of the controversy. This experimentally controversy have motivated several more advanced theoretical model approaches,[13–20] but so far, no final convergence has been reached.[21]

Lithium-like ions in plasma are a few of the most abundant ionic species for specific temperature and density attainable in the laboratory.[22] Various spectroscopic properties of Li-like ions have significant importance in astrophysics due to evidence of high abundances of these ions in different astronomical systems like active galactic nuclei, x-ray binaries, quasars, and hot plasmas.[23,24] For such small-sized atoms, allowed and forbidden transitions with sufficient intensity are used as diagnostic tools of tokamak plasmas.[25–27] For example, there is long literature on the applications of the isolated resonance lines having wavelength 1238.82 Å and 1242.80 Å for N^{4+}, and 1031.91 Å and 1037.61 Å for O^{5+}.[28]

The situation mentioned in the previous paragraph clearly requires extensive and accurate theoretical study of atomic structures. Many interesting results about Li-like ions immersed in plasmas have been reported.[29–39] It was found that for Li-like C^{3+}, N^{4+}, and O^{5+} ions immersed in Debye plasma environment, the oscillator strengths associated with $1s^22s$–$1s^22p$ transitions increase, the transition probabilities associated with $1s^22s$–$1s^23d$ E2 transitions decrease, as the screening strength increases.[33] Base on the code of steady K-shell model for collision radiative balance, Yu *et al.*[34] found that Li-like satellite intensity ratio is density sensitive and temperature unsensitive. The spectral lines corresponding to $\Delta n = 0$ transitions (Here n is the principal quantum number of an atomic state, and $\Delta n = 0$ means that the principal quantum numbers of the two atomic states for one transiton are equal to each other.) for Li-like C^{3+} and Al^{10+} ions show blue-shift, whereas the lines associated to $\Delta n \neq 0$ show red-shift.[35]

*Project supported by the National Natural Science Foundation of China (Grant No. 11847163), the Natural Science Foundation of Gansu Province (Grant No. 20JR10RA131), the Doctoral Science Foundation of Longdong University (Grant No. XYBY202005), the Natural Science Foundation of Shaanxi Province (Grant No. 2021JQ-698), and the Special Project of Department of Education of Shaanxi Province (Grant No. 18JK0710).

†Corresponding author. E-mail: lixf808@163.com

© 2021 Chinese Physical Society and IOP Publishing Ltd

These atomic properties reported in the references mentioned above are general in both weakly and strongly coupled plasmas.

However, Das *et al.*[40] found that $\Delta n = 0$ transitions of Li atom and Li-like Ca^{17+} and Ti^{19+} ions in Debye plasmas, show blue shifts at higher screening lengths and red shifts at lower screening lengths due to the presence of the screenings in the electron–electron interactions. As far as we known, this interesting phenomenon for Debye plasmas was rarely reported, and no cases reported for dense plasmas. The transition properties of Li-like ions ($Z = 7$–11) in dense plasmas are systematically investigated in this work, and it is found that the spectra about $1s^2 3s$–$1s^2 3p$ transitons show first blue-shift and then red-shift with increasing free electron densities.

2. Theoretical method

The transition parameters of Li-like ions ($Z = 7$–11) in dense plasmas are investigated by using the MCDHF method combined with the ion sphere model (ISM). The feasibility of the ISM for describing the dense plasmas screening on atomic structures have been tested by many theoretical research works.[41–50] The MCDHF method and the underlying theories have also been detailly described in many papers.[51–54] Here, only a brief description of the MCDHF and ISM theories is presented.

The wave functions are optimized using the extended optimal level (EOL) version of the MCDHF method. The optimization is on the weighted energy average of the states in EOL scheme. The significant interactions between neighboring levels can be accurately determined by simultaneous optimizing multiple levels with a selected J. A configuration state function (CSF) expansion is generated by the restricted active space method, and excitations from the reference configuration to the active set of orbitals to obtain the jj-coupled CSFs of a given symmetry J and parity P. The active set is defined as a set of orbitals with all orbitals except those common to all CSFs included in the atomic state function (ASF). Single and double substitutions from the multireference set to an active set of orbitals to built the configuration expansions. Electrons from the active space are excited from the occupied orbitals to unoccupied orbitals. Because the orbitals with the same principal quantum number n possess similar energies, to obtain the convergence and stability of atomic parameters, we systematically increase the number of orbitals and expand the size of the active space in layers of principal quantum number n. Only the newly added orbitals are optimized to increase the convergence speed and reduce the processing time. For Li-like ions, the calculated atomic stats are $1s^2 2s$, $1s^2 2p$, $1s^2 3s$, $1s^2 3p$, and $1s^2 3d$, respectively. Initially, the active set (AS) for these atomic stats is

$$\mathrm{AS1} = 3s, 3p, 3d.$$

Then, the active set is increased in the following way:

$$\mathrm{AS2} = \mathrm{AS1} + \{4s, 4p, 4d, 4f\},$$
$$\mathrm{AS3} = \mathrm{AS2} + \{5s, 5p, 5d, 5f\},$$
$$\mathrm{AS4} = \mathrm{AS3} + \{6s, 6p, 6d, 6f\},$$
$$\mathrm{AS5} = \mathrm{AS4} + \{7s, 7p, 7d, 7f\}.$$

The generated orbitals are used to calculate energy eigenvalues and transition parameters. As we separately optimize set of orbitals for the $1s^2 2s$, $1s^2 2p$, $1s^2 3s$, $1s^2 3p$, and $1s^2 3d$ states respectively, we use biorthogonal transformation[55] of the ASFs to calculate transition parameters.

The ISM is based on the following principles: the ion is represented by a point-like nucleus with nuclear charge Z embedded at the center of a spherical cavity containing enough electrons to ensure global neutrality. The spherical cavity is called as an ion sphere or Wigner–Seitz sphere. The ion sphere radius R is determined by the formula

$$4\pi R^3 n_e/3 = Z - N, \tag{1}$$

where n_e is the free electron density, and N is the number of bound electrons. The plasma is assumed to produce an electrically neutral background beyond the ion sphere radius R. For an N-electron atom, the Dirac–Coulomb Hamiltonian containing all of the dominant interactions can be written as

$$H = \sum_{i=1}^{N} H_i + \sum_{i=1}^{N-1} \sum_{j=i+1}^{N} \frac{1}{r_{ij}}, \tag{2}$$

where the first term is the contribution from one-body, and the second term in the sum is the interaction between bound electrons. H_i is defined as

$$H_i = c\boldsymbol{\alpha} \cdot \boldsymbol{p}_i + (\beta - 1)c^2 + V_{\mathrm{IS}}(r_i), \tag{3}$$

where the first and the second terms in Eq. (3) are the relativistic kinetic energy of a bound electron. The last term $V_{\mathrm{IS}}(r_i)$ is effective nuclear potential as "seen" by one bound electron within the ion sphere, and is given by the formula

$$V_{\mathrm{IS}}(r) = \begin{cases} -\dfrac{Z}{r} + \dfrac{Z-N}{2R}\left[3 - \left(\dfrac{r}{R}\right)^2\right], & (r \le R), \\ -\dfrac{N}{r}, & (r > R). \end{cases} \tag{4}$$

The radial wavefunctions of bound electrons are derived by the Dirac equations[56] below

$$\left(\frac{\mathrm{d}}{\mathrm{d}r} + \frac{k}{r}\right) P_{nk}(r) - \frac{1}{c}\left[2c^2 - \varepsilon_{nk} + V_{\mathrm{IS}}(r)\right] Q_{nk}(r) = -X^P(r), \tag{5}$$

$$\left(\frac{\mathrm{d}}{\mathrm{d}r} - \frac{k}{r}\right) Q_{nk}(r) + \frac{1}{c}\left[-\varepsilon_{nk} + V_{\mathrm{IS}}(r)\right] P_{nk}(r) = X^Q(r), \tag{6}$$

where $P_{nk}(r)$ and $Q_{nk}(r)$ are the large and small components of the radial wavefunctions, respectively. Here ε_{nk} is the orbital energy eigenvalue, and n is the principal quantum number. The spin–orbital quantum number $k = -l - 1$ for $j = l + 1/2$, or $k = l$ for $j = l - 1/2$. $X^P(r)$ and $X^Q(r)$ are the "exchange potentials" which force the orthogonality between orbits of the

same symmetry. With regard to the electrically neutral conditions supposed by the ISM, the radial wavefunctions $P_{nk}(r)$ and $Q_{nk}(r)$ are assumed to satisfy the boundary conditions and normalization condition respectively, namely,

$$X(0)=0,\quad X(r)=0,\quad (X=P_{nk}\ \text{or}\ Q_{nk}, r\geq R), \tag{7}$$

$$\int_0^R \left[P_{nk}^2(r)+Q_{nk}^2(r)\right]\mathrm{d}r=1. \tag{8}$$

The ISM mentioned above means that the tested ion is trapped in the center of a hard sphere cavity of radius R, and free electrons are uniformly distributed inside and outside the spherical cavity. That is, if the dense plasma screening effect is described by the ISM, the tested ion will experience both the hard sphere confinement and free electron screening effect.

If a tested ion is trapped in the center of a hard sphere cavity of radius R, and there is nothing in the cavity except the tested ion. The effective nuclear potential as "seen" by one bound electron is given by the formula

$$V_{\mathrm{HS}}(r)=\begin{cases}-\dfrac{Z}{r}, & (r\leq R),\\ \infty, & (r>R).\end{cases} \tag{9}$$

If the surface of the sphere cavity is no longer hard in the ISM, the hard sphere confinement does not exist. That is, a tested ion only experiences free electron screening effect, and the bound electrons can move outside the ion sphere. The boundary conditions and normalization condition of the radial wavefunctions $P_{nk}(r)$ and $Q_{nk}(r)$ are

$$X(0)=0,\quad X(\infty)=0,\quad (X=P_{nk}\ \text{or}\ Q_{nk}), \tag{10}$$

$$\int_0^\infty \left[P_{nk}^2(r)+Q_{nk}^2(r)\right]\mathrm{d}r=1. \tag{11}$$

The other theory for the calculated atomic structures under the hard sphere confinement or free electron screening is the same as that of the ISM mentioned above. All calculations are carried out by using the modified GRASP2K code.[57,58]

3. Results and discussion

3.1. Transition energies and transition probabilities of free Li-like ions

The variations of energy eigenvalues for all Li-like ions ($Z=7$–11) with the active space are the same as each other, so just take the Na^{8+} ion as an example to display the energy eigenvalues change with the active space. It can be seen from Table 1 that the energy eigenvalues of all states become more negative with increasing the active space, and the calculated energy eigenvalues of all states in AS5 space are almost the same as that calculated in AS4 space, namely the energy eigenvalues of all states have converged when the active space is enlarged to the orbital $n=7$.

Table 1. The energy eigenvalues (in unit a.u.) of $1s^22s$ and excited $1s^22p$, $1s^23l$ ($l=0$–2) configurations of Na^{8+} ion as a function of active space. Here, AS1 = 3s, 3p, 3d, AS2 = AS1+{4s, 4p, 4d, 4f}, AS3 = AS2+{5s, 5p, 5d, 5f}, AS4 = AS3+{6s, 6p, 6d, 6f}, AS5 = AS4+{7s, 7p, 7d, 7f}.

Level No.	Configuration	AS1	AS2	AS3	AS4	AS5
1	$1s^22s\ (^2S_{1/2})$	−125.4744	−125.4798	−125.4814	−125.4821	−125.4823
2	$1s^22p\ (^2P_{1/2})$	−124.8153	−124.8228	−124.8248	−124.8255	−124.8257
3	$1s^22p\ (^2P_{3/2})$	−124.8021	−124.8096	−124.8117	−124.8124	−124.8126
4	$1s^23s\ (^2S_{1/2})$	−119.1923	−119.2091	−119.2110	−119.2116	−119.2118
5	$1s^23p\ (^2P_{1/2})$	−119.0027	−119.0281	−119.0312	−119.0320	−119.0322
6	$1s^23p\ (^2P_{3/2})$	−118.9989	−119.0242	−119.0274	−119.0281	−119.0284
7	$1s^23d\ (^2D_{3/2})$	−118.9562	−118.9625	−118.9643	−118.9648	−118.9650
8	$1s^23d\ (^2D_{5/2})$	−118.9551	−118.9614	−118.9632	−118.9637	−118.9639

The transition energies and transition probabilities among $n\leq 3$ transitions of free Li-like ions ($Z=7$–11) are displayed in Table 2. It can be seen from the table that the maximum relative differences between the present calculated transition energies, transition probabilities and those recommended from NIST[59] are 0.78% and 3.46%, respectively. Therefore, it can be concluded that our calculated transition energies and transition probabilities among $n\leq 3$ for free Li-like ions ($Z=7$–11) ions are very accurate, thus the active space of bound electrons of Li-like ions enlarged to the orbital $n=7$ is enough to describe the correlations effect between bound electrons.

3.2. Critical free electron density of $1s^23d$ state

In plasma environment, the number of excited states decreases with the increase of free electron densities due to the effects of IPD. The maximum free electron density that one excited state is effectively bound is called as critical free electron density. The critical free electron density of one state can be obtaiend by the SP model[11] or EK model.[12] When the excitation energy is less than the ionization energy of the lower level state, the upper level state is stable, or else, the upper level state have become quasibound state or disappeared. When the excitation energy is equal to the ionization energy at some free electron density, this free electron density is the critical free electron density that the upper level is effectively bound. In the high-density limit, the formulas of the SP model[11] and EK model[12] used for the IPD of an ion with net charge z are as follows:[60]

$$\Delta I_{\mathrm{sp}}=\frac{3(z+1)}{2R_{\mathrm{sp}}}, \tag{12}$$

$$\Delta I_{\mathrm{ek}}=\frac{z+1}{R_{\mathrm{ek}}}. \tag{13}$$

Table 2. Transition energies E (in unit cm^{-1}) and transition probabilities A (in unit s^{-1}) of free Li-like ions ($Z = 7$–11). The numbers 1, 2, 3, …, 8 represent states, which are the same as expressed in Table 1. Diff (%) denotes the relative difference between the present calculated value and that of NIST.[59] The values x (y) signify $x \times 10^y$.

	N^{4+}						O^{5+}					
	E			A			E			A		
Transition	Present	NIST[59]	Diff (%)	Present	NIST[59]	Diff (%)	Present	NIST[59]	Diff (%)	Present	NIST[59]	Diff (%)
1–2	80511	80463	0.06	3.366(8)	3.37(8)	0.12	96422	96375	0.05	4.087(8)	4.09(8)	0.08
1–3	80816	80722	0.12	3.407(8)	3.40(8)	0.20	97033	96908	0.13	4.169(8)	4.16(8)	0.22
4–5	21655	21639	0.08	4.107(7)	4.10(7)	0.16	26089	26073	0.06	5.049(7)	5.05(7)	0.02
4–6	21746	21715	0.14	4.160(7)	4.14(7)	0.47	26269	26230	0.15	5.157(7)	5.14(7)	0.33
5–7	6641	6639	0.03	8.113(5)	8.11(5)	0.03	8537	8513	0.29	1.195(6)	1.19(6)	0.44
6–7	6551	6562	0.18	1.557(5)	1.57(5)	0.82	8358	8356	0.02	2.242(5)	2.24(5)	0.09
6–8	6573	6584	0.16	9.443(5)	9.49(5)	0.50	8405	8407	0.03	1.369(6)	1.37(6)	0.10
1–5	477825	477766	0.01	1.209(10)	1.21(10)	0.12	666206	666113	0.01	2.609(10)	2.62(10)	0.41
1–6	477915	477842	0.02	1.206(10)	1.21(10)	0.37	666386	666270	0.02	2.601(10)	2.62(10)	0.73
2–4	375659	375663	0.00	3.058(9)	3.04(9)	0.58	543695	543665	0.01	5.719(9)	5.70(9)	0.33
3–4	375353	375405	0.01	6.125(9)	6.07(9)	0.91	543085	543132	0.01	1.147(10)	1.14(10)	0.59
2–7	403955	403941	0.00	3.549(10)	3.55(10)	0.03	578322	578251	0.01	7.319(10)	7.33(10)	0.15
3–7	403650	403682	0.01	7.093(9)	7.09(9)	0.04	577711	577718	0.00	1.462(10)	1.46(10)	0.16
3–8	403672	403704	0.01	4.256(10)	4.26(10)	0.10	577759	577769	0.00	8.774(10)	8.78(10)	0.07
	F^{6+}						Ne^{7+}					
	E			A			E			A		
Transition	Present	NIST[59]	Diff (%)	Present	NIST[59]	Diff (%)	Present	NIST[59]	Diff (%)	Present	NIST[59]	Diff (%)
1–2	112308	112260	0.04	4.805(8)	4.80(8)	0.11	128194	128152	0.03	5.524(8)	5.52(8)	0.07
1–3	113406	113236	0.15	4.954(8)	4.93(8)	0.49	130026	129801	0.17	5.774(8)	5.74(8)	0.60
4–5	30524	30507	0.06	5.994(7)	5.90(7)	1.59	34966	34954	0.04	6.942(7)	6.90(7)	0.61
4–6	30848	30793	0.18	6.191(7)	6.10(7)	1.49	35506	35442	0.18	7.276(7)	7.20(7)	1.06
5–7	10513	10491	0.21	1.638(6)	1.62(6)	1.08	12577	12508	0.55	2.144(6)	2.10(6)	2.10
6–7	10189	10205	0.16	2.981(5)	3.00(5)	0.64	12037	12019	0.15	3.758(5)	3.70(5)	1.57
6–8	10277	10292	0.15	1.836(6)	1.83(6)	0.31	12186	12166	0.16	2.341(6)	2.32(6)	0.91
1–5	885267	885128	0.02	4.960(10)	5.05(10)	1.79	1135055	1134840	0.02	8.611(10)	8.67(10)	0.68
1–6	885590	885414	0.02	4.939(10)	5.03(10)	1.80	1135595	1135328	0.02	8.568(10)	8.64(10)	0.84
2–4	742435	742361	0.01	9.771(9)	9.60(9)	1.78	971895	971734	0.02	1.562(10)	1.55(10)	0.77
3–4	741336	741385	0.01	1.962(10)	1.93(10)	1.64	970063	970085	0.00	3.140(10)	3.10(10)	1.30
2–7	783472	783359	0.01	1.350(11)	1.35(11)	0.30	1019438	1019195	0.02	2.295(11)	2.29(11)	0.21
3–7	782373	782383	0.00	2.696(10)	2.69(10)	0.23	1017606	1017546	0.01	4.582(10)	4.57(10)	0.23
3–8	782461	782470	0.00	1.618(11)	1.61(11)	0.36	1017755	1017693	0.01	2.749(11)	2.74(11)	0.26
	Na^{8+}											
	E			A								
Transition	Present	NIST[59]	Diff	Present	NIST[59]	Diff (%)						
1–2	144099	144062	0.03	6.244(8)	6.23(8)	0.23						
1–3	146980	146688	0.20	6.642(8)	6.60(8)	0.63						
4–5	39418	39420	0.01	7.896(7)	7.93(7)	0.43						
4–6	40267	40180	0.22	8.429(7)	8.40(7)	0.34						
5–7	14745	14630	0.78	2.728(6)	2.68(6)	1.77						
6–7	13896	13870	0.18	4.564(5)	4.56(5)	0.08						
6–8	14135	14070	0.46	2.884(6)	2.85(6)	1.19						
1–5	1415631	1415370	0.02	1.397(11)	1.40(11)	0.22						
1–6	1416480	1416130	0.02	1.388(11)	1.40(11)	0.83						
2–4	1232115	1231888	0.02	2.374(10)	2.31(10)	2.75						
3–4	1229233	1229262	0.00	4.780(10)	4.62(10)	3.46						
2–7	1286277	1285938	0.03	3.666(11)	3.65(11)	0.43						
3–7	1283396	1283312	0.01	7.315(10)	7.27(10)	0.62						
3–8	1283634	1283512	0.01	4.389(11)	4.36(11)	0.67						

The relevant radii are defined by

$$R_{\rm sp}^3 = \frac{3z}{4\pi n_{\rm e}}, \tag{14}$$

$$R_{\rm ek}^3 = \frac{3}{4\pi(n_{\rm e}+n_{\rm i})}, \tag{15}$$

with $n_{\rm e}$ the free electron number density and $n_{\rm i}$ the the ion number density. The atomic unit is used for $\Delta I_{\rm sp}$, $\Delta I_{\rm ek}$, $R_{\rm sp}$, $R_{\rm ek}$, $n_{\rm e}$, and $n_{\rm i}$ in formulas (12)–(15). The conversion factor for number density between atomic unit and cubic centimeter is $1.0\times10^{24}/(0.529)^3$.

In our previous work,[61] we also proposed a new method of estimating the critical free electron density of one state. That is, a bound electron will become a quasibound electron, if the classical turning point radius $R_{\rm ctp}$ of the bound electron is larger than the ion sphere radius R. When $R_{\rm ctp}$ of a bound electron in the highest orbital of one atomic state is equal to R, the corresponding free electron density is the critical free electron density for which the atomic state can be effectively bound. In this work, the selected maximum free electron density for one Li-like ion is equal to the critical free electron density estimated by comparing the classical turning point radius $R_{\rm ctp}$ of 3d electron in $1s^23d$ state and the ion sphere radius R.

The critical free electron densities of $1s^23d$ states for the Li-like ions ($Z=7$–11) are displayed in Table 3. It can be seen from Table 3 that the critical free electron densities $n_{\rm ctp}$ estimated by the classical turning point radius $R_{\rm ctp}$ always greater than those geted by the EK model and SP model, and $n_{\rm ctp}$ is more consistent with $n_{\rm sp}$ which is obtained by the SP model. The critical free electron densities estimated by the classical turning point radius may be little greater, this is caused by the dynamical effects such as the collisions among electrons that are not included in the ISM. If another potential term is added in the ISM to describe the dynamical effects among the electrons, the calculated atomic structure data will be more accurate and will be able to evaluate the IPD effects more effectively.

Table 3. Critical free electron densities (in unit $\rm cm^{-3}$) of $1s^23d$ states for the Li-like ions ($Z=7$–11). $n_{\rm ek}$, $n_{\rm sp}$, and $n_{\rm ctp}$ are the critical free electron densities obtained by the EK model, SP model, and the classical turning point radius, respectively. ΔI is the value of IPD (in unit a.u.) at the critical free electron densities obtained by the EK model or SP model.

Ion	ΔI	$n_{\rm ek}$	$n_{\rm sp}$	$n_{\rm ctp}$
N^{4+}	1.4806	3.35(22)	4.97(22)	6.41(22)
O^{5+}	2.1137	5.88(22)	1.05(23)	1.34(23)
F^{6+}	2.8691	9.52(22)	1.98(23)	2.49(23)
Ne^{7+}	3.7674	1.47(23)	3.50(23)	4.25(23)
Na^{8+}	4.7432	2.10(23)	5.60(23)	6.85(23)

3.3. Energy levels of Li-like ions in dense plasmas

The variation of the energy levels for all states ($n\le3$) of Li-like ions ($Z=7$–11) with free electron densities is similar to that of the Na^{8+} ion, thus here only take the Na^{8+} ion as an example to illustrate the variation of the energy levels with free electron densities. It can be seen from Fig. 1 that the energy levels of $1s^22p$ ($^2P_{1/2,3/2}$) states of the Na^{8+} ion almost linear increase as free electron densities increase, but as shown in Fig. 2 that the energy levels of $1s^23s$, $1s^23p$, and $1s^23d$ states of the Na^{8+} ion decrease with increasing free electron densities. The inner levels which are close to the nucleus experience comparably higher free electron screening effects than those lying near the boundary region[62] [or see Eq. (4)], and the higher angular momentum (l) energy levels having the same principal number (n) experience greater free electron screening effects (see Fig. 4 of Ref. [62]). That is, the greater free electron screening effect is, the higher increase in the energy eigenvalue. The energy eigenvalue that of the ground state $1s^22s$ ($^2S_{1/2}$) is raised by free electron screening, is lower than that of $1s^22p$ ($^2P_{1/2,3/2}$) states, but greater than that of $1s^23s$, $1s^23p$, and $1s^23d$ states. The energy level is the difference between both the energy eigenvalue of excited states and that of ground state. Therefore, as free electron density increases, the energy levels of $1s^22p$ ($^2P_{1/2,3/2}$) states increase, but the energy levels of $1s^23s$, $1s^23p$, $1s^23d$ states decrease.

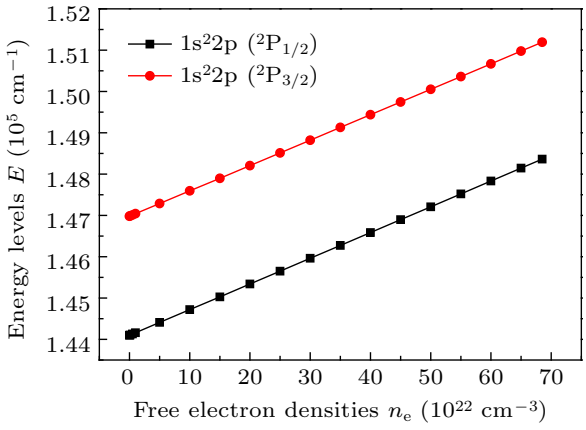


Fig. 1. The variation of the energy levels of $1s^22p$ states of the Na^{8+} ion with free electron densities.

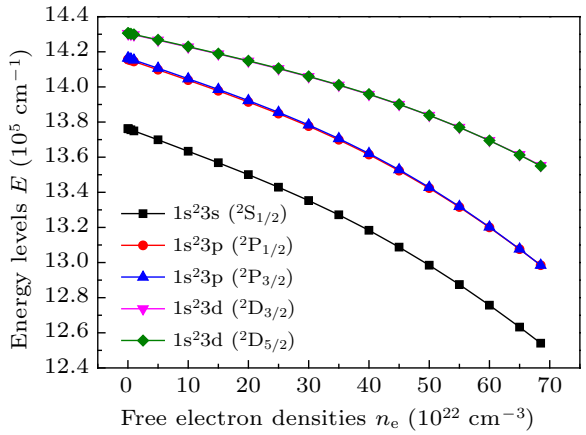


Fig. 2. The variation of the energy levels of $1s^23s$, $1s^23p$, and $1s^23d$ states of the Na^{8+} ion with free electron densities.

3.4. Transition parameters of Li-like ions in dense plasmas

Our calculated transition energies, transition probabilities, weighted oscillator strengths, and line strengths, *etc.*, transition parameters among $n \leq 3$ transitions for Li-like ions ($Z = 7$–11) in dense plasmas are listed in Tables 1–30 of the Supplementary file. These data are important in the feild of plasma diagnosis, astrophysics, and so on. The variation of transition parameters among $n \leq 3$ states of Li-like ions ($Z = 7$–11) with free electron densities are similar to each other. Here only take Na^{8+} ion as an example, to illustrate the transition energies change with free electron densities. The variations of transition energies between all states ($n \leq 3$) of the Na^{8+} ion with free electron densities are displayed in Fig. 3. It can be seen from Fig. 3 that except for $1s^23s$ ($^2S_{1/2}$)–$1s^23p$ ($^2P_{1/2,3/2}$), the spectra corresponding to $\Delta n = 0$ transitions show blue shifts and $\Delta n \neq 0$ transitions exhibit red shifts with increasing free electron densities, and this is similar to that reported in Ref. [35].

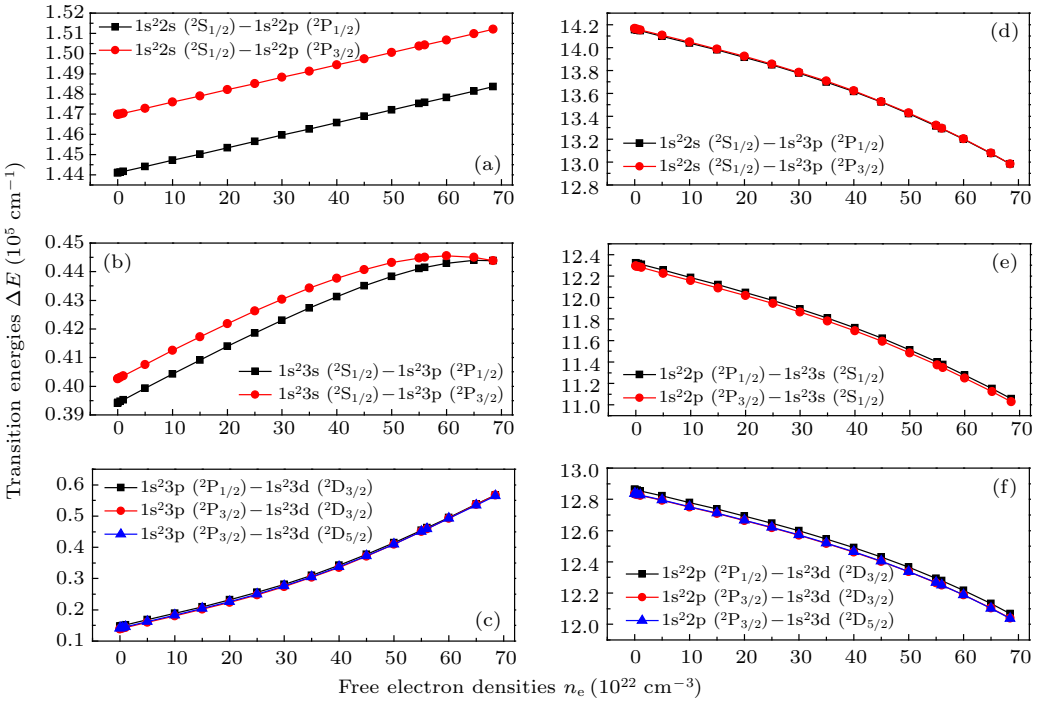


Fig. 3. The variations of the transition energies between all states ($n \leq 3$) of the Na^{8+} ion with free electron densities.

The intensity of plasma screening effect on the atomic structures can also be evaluated by using the transition energy shift, transition probability shift, weighted oscillator strength shift, line strength shift, and so on. The formula of transition energy shift ΔE, transition probability shift ΔA, weighted oscillator strength shift Δgf, and line strength shift ΔS, respectively, are $\Delta E = E_P - E_V$, $\Delta A = A_P - A_V$, $\Delta gf = gf_P - gf_V$, $\Delta S = S_P - S_V$, where E_P, A_P, gf_P, S_P are values of transition energy, transition probability, weighted oscillator strength, and line strength in plasmas, and E_V, A_V, gf_V, S_V are values of transition energy, transition probability, weighted oscillator strength, and line strength in vacuum, respectively. The calculated transition energy shifts, transition probability shifts, weighted oscillator strength shifts, and line strength shifts of different transitions for Li-like ions ($Z = 7$–11) at free electron density 5.0×10^{22} cm^{-3} are listed in Table 31 of the Supplementary file. Figure 4 shows the variation of transition energy shifts *versus* nuclear charge Z at free electron density 5.0×10^{22} cm^{-3}. It can be seen from the figure that the transiton energy shifts of all transitons decrease with increasing nuclear charge Z. This is because in the same free electron density environment, the larger the nuclear charge Z is, the more attractive force the bound electrons experience, which makes the less shift of transiton energy.

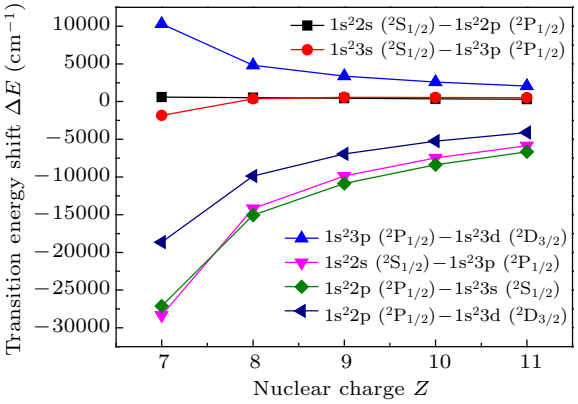


Fig. 4. The variation of transition energy shifts *versus* nuclear charge Z of different transitions for Li-like ions ($Z = 7$–11) at free electron density 5.0×10^{22} cm^{-3}.

It also shows from Fig. 4 that the transiton energy shifts for $\Delta n = 0$ transitions are greater than zero (except for Na^{4+} ion) and those for $\Delta n \neq 0$ transitions are less than zero, this is corresponding to the blue shifts and red shifts of the spectra respectively, which has been mentioned in the previous paragraph. In addition, figure 4 shows that the transition energy

shift of $1s^2 3s(^2S_{1/2})$–$1s^2 3p(^2P_{1/2})$ for the Na^{4+} ion is negative, becasue this transiton has transformed from blue-shift to red-shift, the reason will be discussed in the third paragraph below. The variations of transition probability shift, weighted oscillator strength shifts, and line strength shift change with nuclear charge Z are similar to that of transition energy shift, thus they are not discussed again.

However, it is shown in Fig. 5 that for Li-like ions ($Z = 7$–11), the transition energies of $1s^2 3s$ ($^2S_{1/2}$)–$1s^2 3p$ ($^2P_{1/2,3/2}$) transitions first increase and then decrease with increasing free electron densities, the corresponding spectra show blue shifts at lower free electron densities and red shifts at higher free electron densities. This interesting phenomenon is similar to the reported spectra[40] about $\Delta n = 0$ transitions of Li atom, Ca XVIII and Ti XX ions in Debye screening potential including the electron–electron screening.

It also can be seen from Fig. 5 that the energy level crossings occurs between the $1s^2 3p$ ($^2P_{1/2}$) and $1s^2 3p$ ($^2P_{3/2}$) states of Li-like ions ($Z = 7$–11) as free electron density increase. As can be seen from Fig. 5 that the both free electron densities of spectra changing from blue-shift to red-shift and energy level crossings occuring, increase with increasing nuclear charge Z, and the two free electron densities for the Na^{8+} ion are very close to the critical free electron density of $1s^2 3d$ state.

In dense plasmas, the atomic structures and transition properties of ions are influenced by both the hard sphere confinement and free electron screening, if the dense plasma screening effect is described by the ion sphere model which includes both the hard sphere confinement and free electron screening effect. Take N^{4+} ions as an example, to illustrate the effect of hard sphere confinement and free electron screening on the transition energies of $1s^2 3s$–$1s^2 3p$, respectively. It can be seen from Fig. 6 that the transition energies of $1s^2 3s$ ($^2S_{1/2}$)–$1s^2 3p$ ($^2P_{1/2}$) of the N^{4+} ion decrease with the decrease of hard sphere radius, but increase with increasing free electron density. That is to say, the direction in transition energy changes caused by the hard sphere confinement and free electron screening is opposite. When the N^{4+} ion is immersed in dense plasmas, the transition energies of $1s^2 3s$ ($^2S_{1/2}$)–$1s^2 3p$ ($^2P_{1/2}$) are influenced by both the hard sphere confinement and free electron screening. At lower free electron densities, as the hard sphere radii are relatively larger [see Eq. (1)], the red-shift of transition energy due to hard sphere confinement is less than the blue-shift of transition energy due to free electron screening, thus the transition energies of $1s^2 3s$ ($^2S_{1/2}$)–$1s^2 3p$ ($^2P_{1/2}$) increase with increasing free electron densities. Namely, the spectra of $1s^2 3s$ ($^2S_{1/2}$)–$1s^2 3p$ ($^2P_{1/2}$) show blue shifts at lower free electron densities. However, at higher free electron densities, because the hard sphere radii are relative smaller [see Eq. (1)], the red-shift of transition energy due to hard sphere confinement is greater than the blue-shift of transition energy due to free electron screening, therefore, the transition energies of $1s^2 3s$ ($^2S_{1/2}$)–$1s^2 3p$ ($^2P_{1/2}$) decrease with increasing free electron densities. That is, the spectra of $1s^2 3s$ ($^2S_{1/2}$)–$1s^2 3p$ ($^2P_{1/2}$) show red shifts at higher free electron densities. The reasons about the spectra of $1s^2 3s$ ($^2S_{1/2}$)–$1s^2 3p$ ($^2P_{1/2,3/2}$) transitions for the other Li-like ions ($Z = 7$–11) are similar to that of the N^{4+} ion, thus not repeated again. In addition, it is shown from Fig. 7 that the transition energies of $1s^2 3p$ ($^2P_{1/2}$)–$1s^2 3d$ ($^2D_{3/2}$) of the N^{4+} ion always increase with the decrease of hard sphere radius and increase of free electron density, respectively. Therefore, in dense plasmas, the hard sphere confinement and free electron screening together cause the transition energies of $1s^2 3p$ ($^2P_{1/2}$)–$1s^2 3d$ ($^2D_{3/2}$) of the N^{4+} ion always increase with increasing free electron densities.

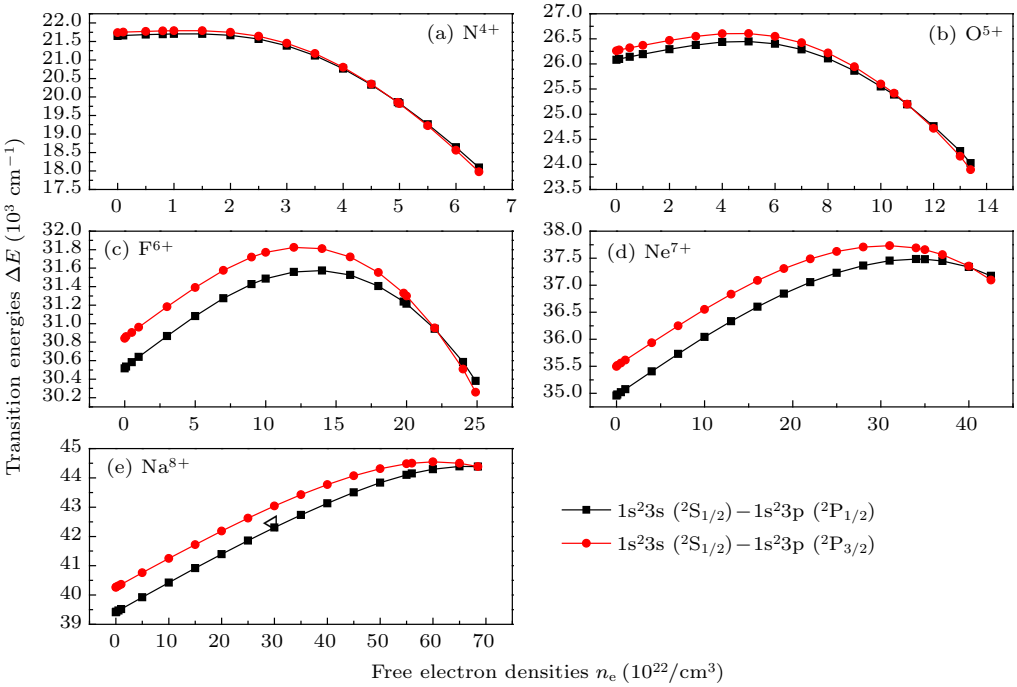


Fig. 5. The variations of $1s^2 3s$–$1s^2 3p$ transition energies of Li-like ions ($Z = 7$–11) with free electron densities.

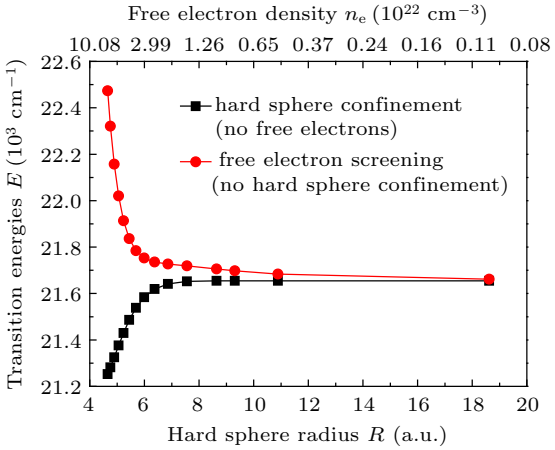


Fig. 6. The variations of $1s^23s$ ($^2S_{1/2}$)–$1s^23p$ ($^2P_{1/2}$) transition energies of N^{4+} ions with hard sphere radius and free electron density.

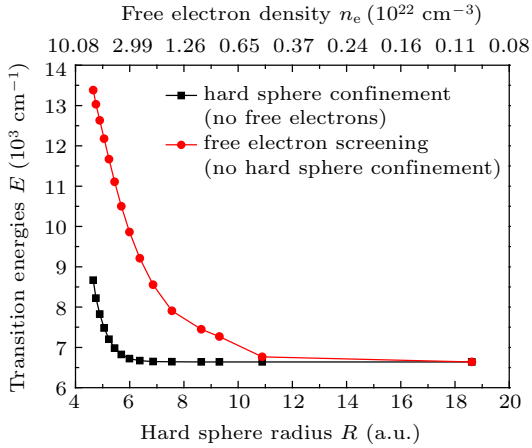


Fig. 7. The variations of $1s^23p$ ($^2P_{1/2}$)–$1s^23d$ ($^2D_{3/2}$) transition energies of N^{4+} ions with hard sphere radius and free electron density.

The phenomenon that the spectra of $1s^23s$ ($^2S_{1/2}$)–$1s^23p$ ($^2P_{1/2,3/2}$) for Li-like ions ($Z = 7$–11) show blue shifts at lower free electron densities and red shifts at higher free electron densities, can be observed in the laboratory. The experimental scheme is as follows. Firstly, all bound electrons in the outer layer of $1s^22s$ specific energy state are ionized by means of laser resonance ionization, so the plasma that mainly contains the ground state $1s^22s$ are obtained. Plasmas with different densities can be obtained by adjusting laser parameters, the initial state of ion-source, and the cavity size. Secondly, the ground state of $1s^22s$ is resonantly excited to the high excited state $1s^23p$ by the method of laser-resonant-transition combined with tuning laser wavelength and power density. Thirdly, the fluorescence wavelengths of $1s^23p \rightarrow 1s^23s$ spontaneous radiation transition are measured by the measurement technology of laser emission spectroscopy, thus the spectra of transition between the two energy states are obtained. Lastly, the red shift or the blue shift of the spectra for $1s^23p$–$1s^23s$ transitions at a certain plasma density can be determined, by comparing the matching relationship between the plasma density parameters and the central wavelength parameters of the fluorescence spectrum. The wavelengths of $1s^23s - 1s^23p$ transitions for Li-like ions ($Z = 7$–11) in dense plasmas are listed in Table 4, and these data have important reference value for future plasma experiments to verify the predicted phenomena that the spectra of $1s^23s$ ($^2S_{1/2}$)–$1s^23p$ ($^2P_{1/2,3/2}$) for Li-like ions ($Z = 7$–11) show blue shifts at lower free electron densities and red shifts at higher free electron densities.

Table 4. Wavelengths (in unit Å) of $1s^23s$–$1s^23p$ transitions for Li-like ions ($Z = 7$–11) in dense plasmas. λ_1 and λ_2 indicate the wavelengths of $1s^23s$ ($^2S_{1/2}$)–$1s^23p$ ($^2P_{1/2}$) and $1s^23s$ ($^2S_{1/2}$)–$1s^23p$ ($^2P_{3/2}$) transitions, respectively. The values $x(y)$ indicate $x \times 10^y$.

N^{4+}			O^{5+}			F^{6+}			Ne^{7+}			Na^{8+}		
n_e	λ_1	λ_2	n_e	λ_1	λ_2	n_e	λ_1	λ_2	n_e	λ_1	λ_2	n_e	λ_1	λ_2
0	4617.87	4598.76	0	3833.18	3806.91	0	3276.11	3241.81	0	2859.92	2816.50	0	2536.98	2483.48
1.00(21)	4616.38	4597.28	1.00(21)	3831.56	3805.32	1.00(21)	3274.93	3240.55	1.00(21)	2859.02	2815.63	1.00(21)	2536.33	2482.87
5.00(21)	4611.70	4592.84	5.00(21)	3825.26	3799.39	5.00(21)	3269.90	3235.83	5.00(21)	2855.43	2812.15	5.00(21)	2533.70	2480.40
8.00(21)	4608.72	4590.31	1.00(22)	3817.67	3791.90	1.00(22)	3263.71	3229.87	1.00(22)	2850.87	2807.88	1.00(22)	2530.43	2477.39
1.00(22)	4607.02	4589.05	2.00(22)	3803.29	3778.15	3.00(22)	3239.81	3207.08	4.00(22)	2824.38	2782.80	5.00(22)	2504.82	2453.45
1.50(22)	4607.02	4589.05	3.00(22)	3790.89	3766.48	5.00(22)	3217.40	3185.63	7.00(22)	2798.77	2758.62	1.00(23)	2473.72	2424.48
2.00(22)	4615.10	4597.70	4.00(22)	3782.72	3759.12	7.00(22)	3197.54	3166.96	1.00(23)	2774.54	2735.75	1.50(23)	2444.15	2396.87
2.50(22)	4636.93	4620.22	5.00(22)	3781.15	3758.41	9.00(22)	3181.98	3152.68	1.30(23)	2752.32	2715.03	2.00(23)	2415.87	2370.68
3.00(22)	4676.39	4661.14	6.00(22)	3787.74	3766.62	1.00(23)	3176.12	3147.62	1.60(23)	2732.02	2696.36	2.50(23)	2389.09	2346.15
3.50(22)	4735.75	4722.77	7.00(22)	3804.02	3784.87	1.20(23)	3168.67	3142.28	1.90(23)	2714.07	2680.46	3.00(23)	2363.90	2323.47
4.00(22)	4816.26	4806.77	8.00(22)	3830.24	3813.88	1.40(23)	3167.16	3143.57	2.20(23)	2698.76	2667.59	3.50(23)	2340.33	2302.87
4.50(22)	4918.60	4913.76	9.00(22)	3866.68	3854.16	1.60(23)	3171.99	3152.39	2.50(23)	2686.08	2657.95	4.00(23)	2318.46	2284.67
4.97(22)	5035.25	5036.77	1.00(23)	3913.89	3906.56	1.80(23)	3184.10	3169.27	2.80(23)	2676.37	2652.03	4.50(23)	2298.64	2269.01
5.00(22)	5043.37	5045.41	1.05(23)	3938.87	3934.37	1.98(23)	3201.33	3191.93	3.10(23)	2670.01	2650.34	5.00(23)	2281.39	2256.62
5.50(22)	5191.57	5202.64	1.10(23)	3969.20	3968.25	2.00(23)	3203.69	3194.89	3.40(23)	2667.88	2653.29	5.50(23)	2267.42	2248.30
6.00(22)	5364.81	5387.64	1.20(23)	4038.94	4045.96	2.20(23)	3231.75	3230.60	3.50(23)	2668.16	2655.62	5.60(23)	2265.01	2247.09
6.41(22)	5527.61	5562.66	1.30(23)	4121.67	4139.07	2.40(23)	3269.68	3277.72	3.70(23)	2670.37	2661.98	6.00(23)	2257.49	2244.77
			1.34(23)	4162.85	4185.15	2.49(23)	3291.64	3304.80	4.00(23)	2678.38	2677.09	6.50(23)	2252.71	2247.19
									4.25(23)	2690.12	2695.71	6.85(23)	2252.91	2252.96

4. Conclusion

In this work, the energy levels, transition energies, transition probabilities, weighted oscillator strengths, and line strengths of Li-like ions ($Z = 7$–11) in dense plasmas are calculated by the MCDHF method combined with the ion sphere model. We find that the active space of bound electrons of Li-like ions is enlarged to the orbital $n = 7$, which is enough to describe the correlations effect between bound electrons. Our calculated transition energies and transition probabilities of free Li-like ions ($Z = 7$–11) agree well with the recommended value of NIST.[59] The critical free electron densities for $1s^2 3d$ states estimated by comparing the classical turning point radius of 3d electrons and the ion sphere radius may be a little greater, this is caused by the dynamical effects such as the collisions among electrons that are not included in the ISM. The energy levels of $1s^2 2p$ states increase, and that of $1s^2 3s$, $1s^2 3p$, and $1s^2 3d$ states of all Li-like ions decrease with increasing free electron densities. Except for $1s^2 3s$ ($^2S_{1/2}$)–$1s^2 3p$ ($^2P_{1/2,3/2}$) transitions, the transition energies of $\Delta n = 0$ transitions increase, and for $\Delta n \neq 0$ transitions decrease with increasing free electron densities.

An interesting phenomenon that the spectra of $1s^2 3s$–$1s^2 3p$ transitions for Li-like ions ($Z = 7$–11) show blue shifts at lower free electron densities and red shifts at higher free electron densities, is predicted at the present work. The reasons are as follows. The dense plasma screening effect is described by the ion sphere model which includes both the hard sphere confinement and free electron screening effect. At lower free electron densities, as the hard sphere radii are relative larger, the red-shift of transition energy due to hard sphere confinement is less than the blue-shift of transition energy due to free electron screening, thus the spectra of $1s^2 3s$–$1s^2 3p$ show blue shifts. However, at higher free electron densities, because the hard sphere radii are relative smaller, the red-shift of transition energy due to hard sphere confinement is greater than the blue-shift of transition energy due to free electron screening, therefore, the spectra of $1s^2 3s$–$1s^2 3p$ show red shifts. This phenomenon can be observed in the laboratory, and the experimental scheme is also given. We hope the phenomenon to be verified by experiment as soon as possible.

Acknowledgment

The authors express sincere gratitude to professor Jönsson P for free providing the GRASP2K program.

References

[1] Das M, Sahoo B K and Pal S 2016 *Phys. Rev. A* **93** 052513
[2] Li X F, Jiang G, Wang H B and Sun Q 2017 *Chin. Phys. B* **26** 013101
[3] Singh N, Goyal A and Chaurasia S 2018 *Radiation Physics and Chemistry* **146** 105
[4] Chen Z B 2019 *Journal of Electron Spectroscopy and Related Phenomena* **236** 12
[5] Li X, Rosmej F B, Lisitsa V S and Astapenko V A 2019 *Phys. Plasmas* **26** 033301
[6] Hoarty D J, Allan P, James S F, *et al.* 2013 *Phys. Rev. Lett.* **110** 265003
[7] Ciricosta O, Vinko S M, Chung H K, *et al.* 2012 *Phys. Rev. Lett.* **109** 065002
[8] Fletcher L B, Kritcher A L, Pak A, *et al.* 2014 *Phys. Rev. Lett.* **112** 145004
[9] Kraus D, Chapman D A, Kritcher A L, *et al.* 2016 *Phys. Rev. E* **94** 011202(R)
[10] Kraus D, Bachmann B, Barbrel B, *et al.* 2019 *Plasma Phys. Control. Fusion* **61** 014015
[11] Stewart J C and Pyatt K D 1966 *Astrophys. J.* **144** 1203
[12] Ecker G and Kröll W 1963 *Phys. Fluids* **6** 62
[13] Vinko S M, Ciricosta O and Wark J S 2014 *Nat. Commun.* **5** 3533
[14] Crowley B J B 2014 *High Energy Density Phys.* **13** 84
[15] Son S K, Thiele R, Jurek Z, Ziaja B and Santra R 2014 *Phys. Rev. X* **4** 031004
[16] Lin C, Röpke G, Kraeft W and Reinholz H 2017 *Phys. Rev. E* **96** 013202
[17] Faussurier G and Blancard C 2018 *Phys. Rev. E* **97** 023206
[18] Rosmej F B 2018 *J. Phys. B: At. Mol. Opt. Phys.* **51** 09LT01
[19] Lin C L, Ropke G, Reinholz H and Kraeft W D 2017 *Contrib. Plasma Phys.* **57** 518
[20] Ropke G, Blaschke D, Dppner T, Lin C, Kraeft W, Redmer R and Reinholz H 2019 *Phys. Rev. E* **99** 033201
[21] Iglesias C A 2014 *High Energy Density Phys.* **12** 5
[22] Kawachi T, Fujimoto T and Csanak G 1995 *Phys. Rev. E* **51** 1428
[23] Nahar S N, Pradhan A K and Zhang H L 2000 *Astrophys. J. Suppl. Ser.* **131** 375
[24] Gorczyca T W, Dumitriu I, Hasoglu M F, Korista K T, Badnell N R, Savin D W and Manson S T 2006 *Astrophys. J. Lett.* **638** L121
[25] Suckewer S, Eubank H P, Goldston R J, McEnerney J, Sauthoff N R and Towner H H 1981 *Nucl. Fusion* **21** 1301
[26] Godefroid M and Fischer C F 1984 *J. Phys. B* **17** 681
[27] Das G C and Sarma 1998 *J. Phys. Plasmas* **5** 3918
[28] Mondal P K, Dutta N N, Dixit G and Majumder S 2013 *Phys. Rev. A* **87** 062502
[29] Aschke L 2000 *Contrib. Plasma Phys.* **40** 72
[30] Xu Z, Fan P, Zhang Z, Chen S, Lin L,Lu P, Wang X, Qian A, Yu J, Sun L and Wu M 1990 *Appl. Phys. Lett.* **56** 2370
[31] Boiko V A, Brunetkin B A, Faenov A Y, Hahalin S Y, Skobelev I Y and Shilov K A 1984 *Phys. Scr.* **30** 59
[32] Peng F, Jiang G and Zhu Z H 2006 *Chin. Phys. Lett.* **23** 3245
[33] Mondal P K, Dutta N N, Dixit G and Majumder S 2013 *Phys. Rev. A* **87** 062502
[34] Yu X M, Cheng S B, Yi Y G, Zhang J Y, Pu Y D, Zhao Y, Hu F, Yang J M and Zheng Z J 2011 *Acta Phys. Sin.* **60** 085201 (in Chinese)
[35] Madhulita D, Chaudhuri R K and Chattopadhyay S 2012 *Phys. Rev. A* **85** 042506
[36] Lee R W, Matthews D L and Scofield J 1981 *J. Phys. B: At. Mol. Phys.* **14** 3079
[37] Qi Y Y, Wu Y and Wang J G 2009 *Phys. Plasmas* **16** 033507
[38] Sahoo S and Ho Y K 2006 *Phys. Plasmas* **13** 063301
[39] Mehdipour M, Kaastra J S and Raassen A J J 2015 *Astronomy & Astrophysics* **579** A87
[40] Das M, Sahoo B K and Pal S 2014 *J. Phys. B: At. Mol. Opt. Phys.* **47** 175701
[41] Ichimaru S 1982 *Rev. Mod. Phys.* **54** 1017
[42] Li X F and Jiang G 2018 *Chin. Phys. B* **27** 073101
[43] Bhattacharyya S, Saha J K and Mukherjee T K 2015 *Phys. Rev. A* **91** 042515
[44] Sil A N, Anton J, Fritzsche S, Mukherjee P K and Fricke B 2009 *Eur. Phys. J. D* **55** 645
[45] Salzmann D and Szichman H 1987 *Phys. Rev. A* **35** 807
[46] Saha B and Fritzsche S 2007 *J. Phys. B: At. Mol. Opt.* **40** 259
[47] Li Y Q, Wu J H, Hou Y and Yuan J M 2009 *J. Phys. B: At. Mol. Opt. Phys.* **42** 235701
[48] Li X, Xu Z and Rosmej F B 2006 *J. Phys. B: At. Mol. Opt. Phys.* **39** 3373

[49] Li Y Q, Wu J H, Hou Y and Yuan J 2008 *J. Phys. B: At. Mol. Opt. Phys.* **41** 145002
[50] Li X F, Jiang G, Wang H B and Sun Q 2017 *Chin. Phys. B* **26** 013101
[51] Grant I P, McKenzie B J, Norrington P H, Mayers D F and Pyper N C 1980 *Comput. Phys. Commun.* **21** 207
[52] Dyall K G, Grant I P, Johnson C T, Parpia F A and Plummer E P 1989 *Comput. Phys. Commun.* **55** 425
[53] Grant I P 1970 *Adv. Phys.* **19** 747
[54] Chen Z, Sang C and Wang K 2019 *Journal of Quantitative Spectroscopy & Radiative Transfer* **225** 76
[55] Olsen J, Godefroid M R, Jönsson P, Malmqvist P and Fischer C F 1995 *Phys. Rev. E* **52** 4499
[56] Grant I P 1994 *Comput. Phys. Commun.* **84** 59
[57] Jönsson P, Gaigalas G, Bieroń J, Fischer C F and Grant I P 2013 *Comput. Phys. Commun.* **184** 2197
[58] Jönsson P, He X, Fischer C F and Grant I P 2007 *Comput. Phys. Commun.* **177** 597
[59] https://www.nist.gov/pml/atomic-spectra-database
[60] Iglesias C A and Sterne P A 2013 *High Energy Density Phys.* **9** 103
[61] Li X, Zheng X, Deng P and Jiang G 2018 *Eur. Phys. J. D* **72** 176
[62] Madhulita D, Madhusmita D, Rajat K C and Sudip C 2012 *Phys. Rev. A* **85** 042506